State-to-State Cross Sections for Rotationally Inelastic Collision of He with Na_2

Y. Wang*

Department of Electrical Engineering, Tongling University, Tongling, 244000, China

(Received September 19, 2010)

As a further theoretical study of the collision-induced quantum interference on rotational energy transfer in an atom–diatom system, the differential interference angles for singlet-triplet mixed states of Na_2 system in collision with He were calculated based on the first-Born approximation of time-dependent perturbation theory, taking into account the anisotropic Lennard–Jones interaction potential and the long-range interaction potential. The relationships of differential interference angle versus impact parameter including collision parameter, velocity, are obtained. It is beneficial to reduce the loss in molecular cooling and trapping.

PACS: 34.20.−b

1. Introduction

Collisional energy transfer in weakly interacting molecule has been the subject of numerous experimental and theoretical studies [1] because of the importance of such processes in several areas of molecular physics and chemical physics. On the other hand, the relevant state-to-state cross sections with which the actual energy content of the heat bath can be collisionally transferred to different molecular degrees of freedom, and the various external conditions which control the relative weights of the final inelastic channels, provide an essential piece of information. Recent progress in the development of experimental methods for the cooling and trapping of atoms and molecules may provide an opportunity for high resolution spectroscopy, accurate determination of intermolecular potentials, and the study of reactive and inelastic collisions at ultralow temperatures [2, 3]. Several methods have been proposed for creating translationally cold molecules with thermal or nonthermal vibrational excitation. They rely on removing kinetic energy from molecules one way or another. A successful demonstration of trapping CaH in a magnetic field with the buffer gas loading technique was carried out by Weinstein et al. [4]. Here, a cold buffer gas of ^{3}He is used to cool molecules to a temperature of about 240 mK. Molecules, slowed down by elastic collisions with the buffer gas, are trapped in an inhomogeneous magnetic field. In the context of the buffer gas loading experiment, there are several *ab initio* calculations for different van der Waals complexes of He atoms and diatomic molecules: He + H_2, He + O_2, He + CO, He + CaH, He + NH, He + F_2, He + N_2, etc. [5]. These studies have provided accurate intermolecular potential for these complexes and have given new insight into the behavior of atom–diatom collisions at ultracold temperatures including investigations of the Feshbach resonances, predissociation in the Van der Waals complexes, determination of complex scattering lengths, testing of effective range theory and the Wigner threshold laws, and quasiresonant vibration–rotation energy transfer.

On the other hand, alkali metal dimers are of great interest to both theoreticians and experimentalists, because they are theoretically tractable and their experimental properties can be observed with various techniques. During the past few years this interest has increased mainly due to the observation of the photoassociation of cold alkali atoms [6] and their Bose condensation. So currently there is an explosion of interest in the structure and properties of sodium clusters [7]. Attention focuses not only on the properties of the cluster but also on its interactions with other atoms, molecules, or clusters [8]. The interactions between Na_2 and the rare gas atoms have also attracted much attention. Up to date there have already several studies made on the He–Na_2 system. In 1971 Krauss et al. [9] first published a model potential [10], which is based on a Hartree–Fock potential curve for He–Na. Then at 1981 Schinke [11] used a single set of Gaussian-type orbital for the whole surface. For each sodium atom, 11s and 5p functions contracted to [7s, 4p] were employed, and for helium atom, 7s and 2p functions contracted to [4s, 2p] were used. They predict the well depth to be 0.8066 cm^{-1}. The basis sets which they used might not be big enough for such shallow well depth. All the potential energy surfaces (PESs) calcu-

* e-mail: wangyue8001@sohu.com

lated before for title system are either semiempirical or obtained by fitting preexisting but old *ab initio* calculations. In this article we used the new three-dimensional He–Na_2 interaction potential [12]. Based on the fitted PES state-to-state differential cross sections (DCSs), integral cross sections are calculated.

2. Potential energy surface and computational method

2.1. Potential energy surface

In Ref. [12] the main features of the potential may be summarized as below:

(1) The PES has two shallow wells corresponding to the T-shaped structure and the linear configuration. For the linear configuration of well located at $14a_0$, the well depth is 1.584 cm^{-1} and the T-shaped structure corresponds to $12.5a_0$, the well depth is 1.769 cm^{-1}. The whole PES exhibits weak anisotropy (shown in Fig. 1).

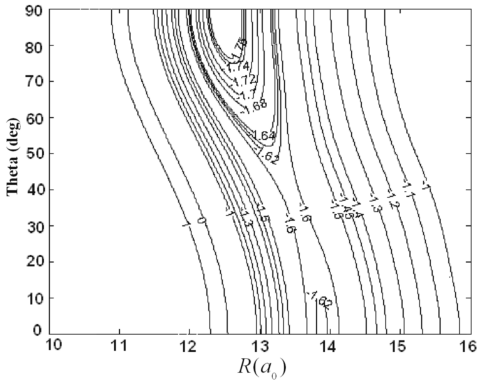

Fig. 1. Contour plots of the potential for He–Na_2 complex at $r = r_e$. Contours are labeled in cm^{-1}.

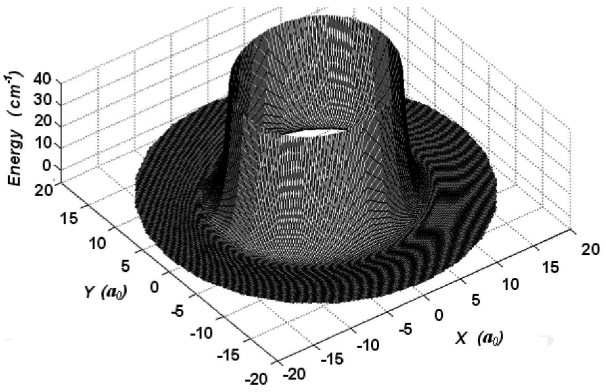

Fig. 2. 3D view of the interaction potential for He–Na_2 complex at $r = 5.8175a_0$.

(2) The interaction potential has high angular anisotropy, similar to the He–Li_2 system. In Fig. 2 we show a 3D view of global behavior of this new PES at $r = 5.8175a_0$. In this figure, one can easily see the mainly isotropic interaction and the well-defined molecular core identified by the repulsive regions which show vanishing angular dependence for this very weakly bound Van der Waals complex.

2.2. The quantum dynamics

In our work we implement the close coupling calculation for rotationally inelastic collision of Na_2 with He. This may be done either in a body-fixed frame [13] or in a space-fixed (SF) [14] frame. In order to obtain the experimental observations such as DCS and temperature--dependent rate constant, the SF frame is a favorable one. We use the conventional Jacobi coordinates (R, r, θ), where r is the bondlength of Na–Na (fixed at its equilibrium value, $5.8175a_0$), R is the separation of the atom He and the center of mass of Na–Na and θ is the enclosed angle, $\theta = 0°$ corresponds to the collinear He–Na_2 geometry. The total scattering wave function is expanded as

$$\psi_{jl}^{JM}(\hat{R}, \hat{r}) = \sum_{j'l'} R^{-1} u_{j'l'}^{Jjl}(R) \phi_{j'l'}^{JM}(\hat{R}, \hat{r}) \,, \tag{1}$$

where J denotes the total angle momentum, j is the rotational angular momentum for Na_2, and l is the orbital angular momentum.

As we easily see from Eq. (1), the presence of the two sets of asymptotic indices (jl) and $(j'l')$ prepares for a representation of the effect of the anisotropic potential which will couple the initial state (jl) to the final state $(j'l')$ reached after the collision. Substitution of expansion (1) into the stationary Schrödinger equation, the close coupling calculation equations for the radial coefficients $u_{j'l'}^{Jjl}$ became

$$\left[\frac{\mathrm{d}^2}{\mathrm{d}R^2} + k_{jj'}^2 - \frac{l'(l'+1)}{R^2}\right] u_{j'l'}^{Jjl}(R) = 2\mu \sum_{j''l''} \langle j'l' | \, V(R,\theta) \, | j''l'' \rangle \, u_{j'l'}^{Jjl}(R) \,. \tag{2}$$

Here

$$k_{jj'}^2 = 2\mu(E_{\mathrm{col}} + \varepsilon_{\mathrm{rot}}^{j} - \varepsilon_{\mathrm{rot}}^{j'}) \,, \tag{3}$$

where E_{col} is the collision energy, $\varepsilon_{\mathrm{rot}}^{j}$ and $\varepsilon_{\mathrm{rot}}^{j'}$ is the initial and the final rotational energy level of the Na–Na, respectively. In order to evaluate the potential energy matrix elements the interaction potential is conventionally expanded in the Legendre polynomials

$$V(R,\theta) = \sum_{\lambda} V_\lambda(R) P_\lambda(\cos\theta) \tag{4}$$

and the integrals $\langle j'l'|V(R,\theta)|j''l''\rangle$ are subsequently taken analytically [15].

The coupled Eqs. (3) are solved numerically. Matching the solutions to the proper boundary conditions for the radial wave function $(u_{j'l'}^{Jjl})$ in the asymptotic region leads to the transition matrix elements $T_{jl\to j'l'}^{J}$, and the scattering amplitude is taken as [16]:

$$f_{jm_j\to j'm'_j}(\hat{R}) = \left(\frac{\pi}{k_j k_{j'}}\right)^{1/2} \times \sum_{JMll'm_{l'}} i^{l-l'+1}(2l+1)^{1/2}(j'm_{j'}l'm_{l'}|j'l'JM) \times T^J_{jl\to j'l'}(jlm_j0|jlJM)Y_{l'm_{l'}}(\hat{R})\,, \quad (5)$$

from which the DCSs for the $j \to j'$ transition averaged over initial m_j and summed over final $m_{j'}$ projections, are

$$\frac{\mathrm{d}\sigma_{j\to j'}}{\mathrm{d}\Omega} = \frac{k_{j'}}{(2j+1)k_j}\sum_{m_j m_{j'}}\left|f_{jm_j\to j'm_{j'}}\right|^2. \quad (6)$$

The total cross section are given by the usual formulae

$$\sigma_{j\to j'} = \sum_J P^J_{j\to j'}. \quad (7)$$

Here, $P^J_{j\to j'}$ are the partial cross sections

$$P^J_{j\to j'} = \frac{(2J+1)\pi}{(2j+1)k_j^2}\sum_{ll'}\left|T^J_{jl\to j'l'}\right|^2. \quad (8)$$

Since the T matrix goes to zero for large J, this sum will converge and can be truncated.

3. Results and discussion

In our work all calculations used the hybrid modified log-derivative Airy propagator [17, 18] to solve the close coupling (CC) equations and obtain rotationally inelastic cross sections. Thirty-two point Gauss–Legendre quadrature was adopted to evaluate the expansion coefficients $V_\lambda(R)$ in Eqs. (4), and the Legendre terms up through $\lambda_{\max} = 12$ were included. The results were checked by reasonable changes in propagator step size, the maximum distance for the propagation and the total number of rotational states included in the basis.

3.1. Differential cross-sections

We try first to understand some features of the He–Na_2 collision by looking at inelastic DCSs. A crossed molecular beam experiment can directly measure the DCS; the number of rovibrationally selected Na_2 molecule striking a finite size detector at a fixed scattering angle will be proportional to the DCS. In Fig. 3 we show the computed state-to-state rotational DCS of He–Na_2 system from the initial $j = 0$ at a collision energy of 90 meV (726 cm^{-1}) (refer to the $j = 0$ rotational level of Na_2 molecule). The fast narrow diffraction oscillations in the cross sections are the obvious characters for the low Δj inelastic transitions, and decrease with j' increasing. It was well known they happen as a result of the interference of quantum mechanical waves associated with different classical trajectories leading to the same scattering angle and the same angular momentum transfer. The largest amplitude occurs at small scattering angles. There is very little backward scattering. This suggests that in a low Δj transition, the He projectile is predominantly forward scattered in the molecular frame of reference. We suggest that the scattering pattern in Fig. 3 will be typical for systems in which the usual rainbow maximum is absent and only pure orientation interferences arise.

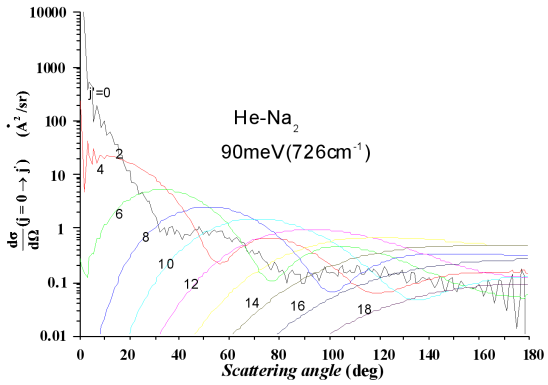

Fig. 3. CC differential cross sections for selected rotational excitation $j = 0 \to j'$ transitions versus scattering angle θ. The collision energy is 90 meV.

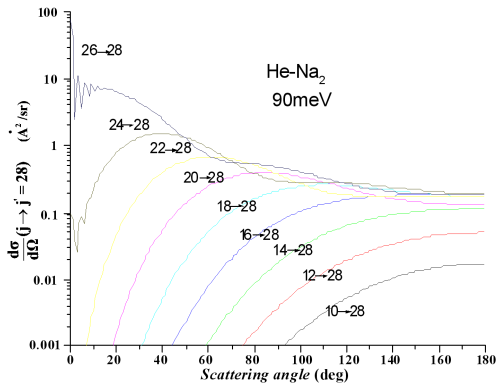

Fig. 4. CC differential cross sections for selected $j \to j' = 28$ transitions versus scattering angle θ. The collision energy is 90 meV.

cross sections at the collision energy of $E = 90$ meV with $j' = 28$ and selected initial states are plotted in Fig. 4. The overall behavior is similar to the corresponding $0 \to j'$ transitions in Fig. 3; the rotational rainbow oscillations, however, are strongly quenched and only slightly indicated even for the $\Delta j = 2$ transition. Therefore, state-to-states cross sections starting out of low rotational states, ideally the ground state $j = 0$, should be considered in future experiments to resolve these rotational rainbow oscillations.

Because of some substantial deviations in Fig. 5, especially for higher transition, we perform a diminished comparison and normalize each experimental cross section curve separately to the theoretical one. Thus, only the angular dependences of the individual Δj transitions are considered. Surprisingly, the agreement for $\Delta j = 0$

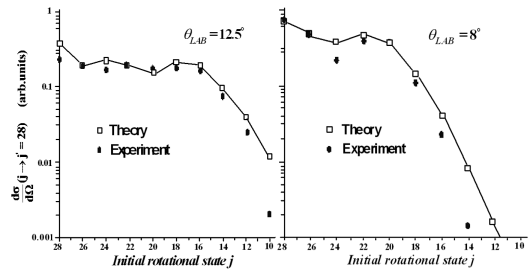

Fig. 5. Comparison between theoretical and experimental differential cross sections for $j \to j' = 28$ transitions at $\theta_{\mathrm{LAB}} = 12.5°$ and 8°. The collision energy is 90 meV.

($j = 28 \to 28$) is rather poor. However, this artifact does not affect the inelastic cross sections and excellent agreement is obtained for the $\Delta j = 2$ ($j = 26 \to 28$) transition. The small shoulder at $\theta_{\mathrm{LAB}} = 8°$, which reminds one of a rotational rainbow oscillation, is also observed in the experimental cross section curve [19], The theoretical cross sections are overestimated around the rotational rainbow maximum and in the classically forbidden region, where the theoretical cross sections fall off too slowly. This is expected to be valid for the He–Na_2 system because the potential well depth is very shallow.

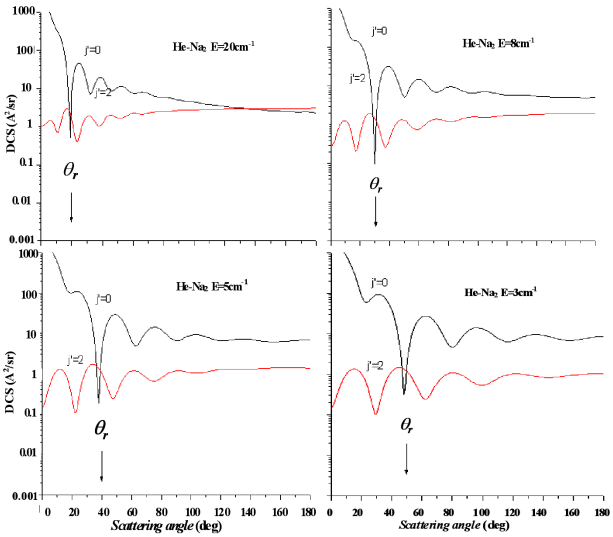

Fig. 6. Differential cross sections for selected $j = 0 \to j' = 0, 2$ transitions versus scattering angle θ. The collision energy is 3 cm^{-1}, 5 cm^{-1}, 8 cm^{-1}, 20 cm^{-1}, respectively.

Inspecting Fig. 6 we compared with four different low collision energies (the collision energy is 3 cm^{-1}, 5 cm^{-1}, 8 cm^{-1}, 20 cm^{-1}, respectively) for $j = 0 \to j' = 0, 2$ transitions versus scattering angle θ. In this figure, we can observe that with a decrease in energy the rotational rainbow maxima (θ_{r}) move to the larger angle by an alternation about $\Delta\theta = 10°$. This is because of purely repulsive potentials, the previous studies [20–22] showed that the angular distributions of inelastic DCS provide a useful visualization of rotational rainbows, they present the following typical characteristics: they are "dark", less intense, on the low angle side of the rainbow. When the higher Δj inelastic transitions are considered, it is obviously not the case described above. It is therefore reasonable to suggest that attractive well and low energies play a considerable role in low Δj inelastic collisions.

3.2. Integral cross-sections

The inelastic $j = 0, 1 \to j'$ integral cross sections are displayed graphically in Fig. 7. Due to the integration over the scattering angle rotational rainbow oscillations characteristic to DCSs are not observed [23]. All distributions show the same typical behavior. The onset of the rapidly decreasing branch at larger transitions shifts further out with increasing energy. Similar final state distributions were reported by Jendrek and Alexander [24] for He–LiH collisions using the coupled-states approximation.

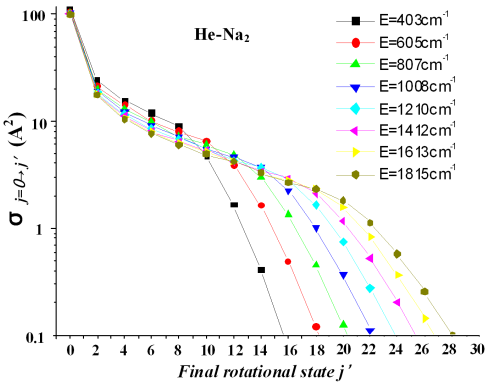

Fig. 7. Integral cross sections for $j = 0 \to j'$ transitions versus final rotational state j'.

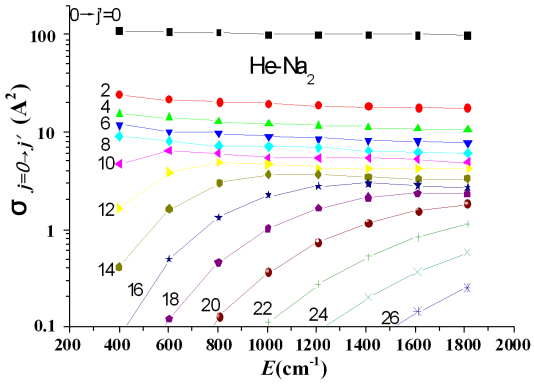

Fig. 8. Integral cross sections for $j = 0 \to j'$ transitions versus collision energy E.

In Fig. 8 the energy dependence of selected integral cross sections is investigated for 403 cm^{-1}(0.05 eV) $\leq E \leq$ 1815 cm^{-1}(0.25 eV). In this energy range the

$j = 0 \rightarrow j' = 0, 4$, and 8 cross sections decrease slowly with E, while those for the higher transitions rise steeply at lower energies, reach a broad maximum, and decrease finally with almost the same gradient as the elastic one. The maximum shifts to larger energies for higher transitions. The energy that depended on single rotational excitation cross sections as shown in Fig. 8 have been also observed in numerous theoretical studies mainly concerning the systems such as He–H_2 [25, 26] and H–H_2 [27]. In the present case they are easily understood in the context of rotational rainbows or, likewise, classically allowed and forbidden transitions.

4. Conclusions

In this work we have employed a newly computed PES to study various state-to-state cross sections of the rotationally inelastic excitation of Na_2 molecule by collision with He atom. The close coupling method is adopted. DCSs show the feature of forward scattering for low Δj inelastic transitions and backward scattering for high Δj transitions at the energy examined. The long-range attractive well gives the significant contribution to the partial cross section for $j = 0 \rightarrow j' = 1, 2$ inelastic transitions, whereas it does not exist for the higher inelastic transitions. The dependence of the integral cross sections on j' from $j = 0, 1$ is not monotonic but displays a pronounced oscillatory structure, which proves to be a sensitive probe of the interaction potential, and the dependence on low collision energy presents resonance features. We relate these features with the anisotropic interaction potential in detail. This work should provide useful information for further experimental and theoretical studies.

References

[1] L.H. Kang, B. Dai *Can. J. Chem.* **88**, 453 (2010).

[2] R.V. Krems, *Int. Rev. Phys. Chem.* **25**, 283 (2006).

[3] H.L. Bethlem, G. Meijer, *Int. Rev. Phys. Chem.* **22**, 73 (2003).

[4] J.R. Weinstein, R. deCarvalho, T. Guillet, B. Friedrich, J.M. Doyle, *Nature* **395**, 148 (1998).

[5] E. Bodo, F.A. Gianturco, *Int. Rev. Phys. Chem.* **25**, 313 (2006).

[6] V. Kokouline, O. Dulieu, R. Kosloff, F. Masnow--Seews, *J. Chem. Phys.* **110**, 9865 (1999).

[7] K.D. Bonin, V.V. Kresin, *Electric Dipole Polarizabilities of Atoms, Molecules and Clusters*, World Sci., Singapore 1997.

[8] V.V. Kresin, G. Tikhonov, V. Kasperovich, K. Wong, P. Brockhaus, *J. Chem. Phys.* **108**, 6660 (1998).

[9] M. Krauss, P. Maldonado, A.C. Wahl, *J. Chem. Phys.* **54**, 4944 (1971).

[10] E. Berbenni, P. McGuire, *Chem. Phys. Lett.* **45**, 84 (1977).

[11] R. Schinke, W. Müller, W. Meyer, P. McGuire, *J. Chem. Phys.* **74**, 3916 (1981).

[12] Y. Wang, W.Y. Huang, E.Y. Feng, Z.F. Cui, *Sci. China B* **51**, 539 (2008).

[13] J.M. Launay, *J. Phys. B, At. Mol. Opt. Phys.* **10**, 3665 (1977).

[14] A.M. Arthurs, A. Dalgarno, *Proc. R. Soc. A* **256**, 540 (1960).

[15] F.A. Gianturco, S. Kumar, S.K. Pathak, M. Raimondi, M. Sironi, *Chem. Phys.* **215**, 239 (1997).

[16] W.H. Miller, *Dynamics of Molecular Collisions*, Vol. I, Plenum Press, New York 1976, p. 13.

[17] D.E. Manolopoulos, M.H. Alexander, *J. Chem. Phys.* **86**, 2044 (1987).

[18] M.H. Alexander, *J. Chem. Phys.* **81**, 4510 (1984).

[19] K. Bergmann, U. Hefter, J. Witt, *J. Chem. Phys.* **72**, 4777 (1980).

[20] L.J. Rawluk, Y.B. Fan, Y. Apelblat, M. Keil, *J. Chem. Phys.* **94**, 4205 (1991).

[21] F.A. Gianturco, A. Palma, *J. Chem. Phys.* **83**, 1049 (1985).

[22] P.F. Vohralik, R.E. Miller, R.O. Watts, *J. Chem. Phys.* **90**, 2182 (1988).

[23] R. Schinke, *J. Chem. Phys.* **72**, 1120 (1980).

[24] E.F. Jendrek, M.H. Alexander, *J. Chem. Phys.* **72**, 6452 (1980).

[25] J.L. Nolte, B.H. Yang, P.C. Stancil, *Phys. Rev. A* **81**, 014701 (2010).

[26] Q.F. Chen, L.C. Cai, *Int. J. Thermophys.* **27**, 437 (2006).

[27] A.N. Panda, K. Giri, N. Sathyamurthy, *J. Phys. Chem. A* **109**, 2057 (2005).